Spin dynamics in InAs nanowire quantum dots coupled to a transmission line

Mircea Trif, Vitaly N. Golovach, and Daniel Loss
Department of Physics, University of Basel, Klingelbergstrasse 82, CH-4056 Basel, Switzerland
(Received 19 August 2007; published 31 January 2008)

We study theoretically electron spins in nanowire quantum dots placed inside a transmission line resonator. Because of the spin-orbit interaction, the spins couple to the electric component of the resonator electromagnetic field and enable coherent manipulation, storage, and readout of quantum information in an all-electrical fashion. Coupling between distant quantum-dot spins, in one and the same or different nanowires, can be efficiently performed via the resonator mode either in real time or through virtual processes. For the latter case, we derive an effective spin-entangling interaction and suggest means to turn it on and off. We consider both transverse and longitudinal types of nanowire quantum dots and compare their manipulation time scales against the spin relaxation times. For this, we evaluate the rates for spin relaxation induced by the nanowire vibrations (phonons) and show that, as a result of phonon confinement in the nanowire, this rate is a strongly varying function of the spin operation frequency and thus can be drastically reduced compared to lateral quantum dots in GaAs. Our scheme is a step forward to the formation of hybrid structures where qubits of different nature can be integrated in a single device.

DOI: 10.1103/PhysRevB.77.045434 PACS number(s): 73.63.Kv, 73.63.Nm, 72.25.Rb

I. INTRODUCTION

Over the last decade, the spin of individual electrons in semiconductor nanostructures has been intensively studied in relation to spin-based quantum computing schemes.[1–3] Attaining an almost full control over the spin of individual electrons in quantum dots (QDs) opens the possibility to study single-spin dynamics in a solid state environment in the presence of relaxation and decoherence. Although lateral or two-dimensional QDs (2D) have been most successfully used until now to demonstrate spin coherence and usability for quantum computing,[2,3] novel quantum systems have emerged in recent years, providing a number of new ways to implement the basic ideas of quantum computing.[4] Among such systems are the QDs formed inside semiconductor nanowires.[5,6]

Rapid progress in GaAs nanostructures started once few-electron QDs became available (for a review, see, e.g., Ref. 7), which opened the door to control the number of electrons in a single QD down to one in vertical[8] and lateral[9] dots, as well as in double QDs.[10–12] Further important experimental progress came with the advent of charge sensors which, quite remarkably, enabled the measurement of the relaxation time of one single spin.[13] The longest spin relaxation times in single GaAs QDs extend up to several seconds[14] and were measured in lateral dots at relatively small magnetic fields ($B \sim 1$ T).

The spin decoherence time in GaAs was measured also in double QDs by studying the hyperfine-induced mixing of singlet and triplet states.[15,16] In the same setup, a universal entanglement operation was implemented,[16] enabling a square-root-of-swap operation[1] between two spin-1/2 qubits on a time scale of 180 ps. Resonant and coherent manipulation of a single spin-1/2 has recently been implemented in a GaAs double QD, making use of electron spin resonance[17,18] (ESR) as well as electric-dipole induced spin resonance[19,20] (EDSR) techniques. Resonant but incoherent (hyperfine-mediated) spin manipulation in double dots was also recently demonstrated.[21]

The use of different semiconductors, other than GaAs, has since long been a pursuit with the goal to create nanostructures with novel properties. Particular examples are InAs and InP nanowires, where both gate-defined and "barrier" defined QDs could be fabricated.[22–25] The advantage of these materials is that both optical and transport measurements can be carried out on the same type of structure. The number of electrons can equally well be controlled down to one electron per dot,[23] which shows that QDs created in nanowires can serve as alternative candidates for spin qubits.

One particular difference between GaAs and InAs semiconductors is the strength of the spin-orbit interaction (SOI), which is much larger for the latter material. This fact, however, is a double-edge sword; on one hand, it opens up the possibility to efficiently manipulate the electron spin with *electric* fields only,[20,26–29] while, on the other hand, it implies stronger coupling of the spin to charge environments, such as phonons, particle-hole excitations, gate voltage fluctuation, etc. However, due to the quasi-one-dimensional structure of the nanowires, the spin relaxation times due to phonons and SOI turn out to be longer than one might expect from QDs created in InAs bulk material. Indeed, the time scales obtained in this work are on the order of microseconds to milliseconds for sufficiently large Zeeman splittings. At the same time, the relaxation rate exhibits peaks as a function of a static applied magnetic field due to the quantization of the phonon spectrum. The long relaxation time and the presence of a sizable SOI permit then an efficient control of coherent spin states by making use of EDSR.[19,20,26–28]

One of the main ingredients in the spin-qubit scheme[1] is the electrical control of two-qubit gates to generate entanglement. While the original proposal involved only local interactions between neighboring spins, it is desirable to couple spins directly over large distances, since this produces a better threshold for fault tolerant quantum computation.[30] A solution to this problem was first proposed in Ref. 31 and involves optical cavities whose photon modes mediate interaction between distant spins. The coupling of the spin to

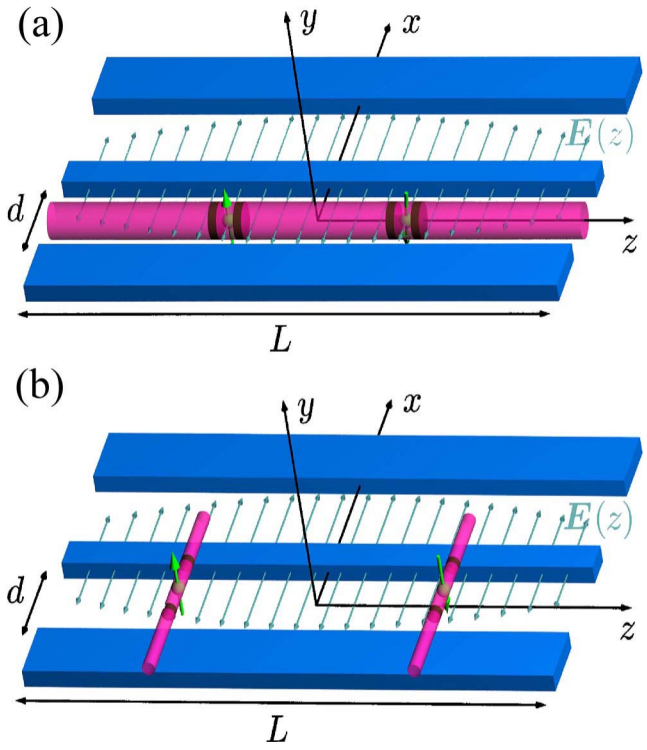

FIG. 1. (Color online) Schematics of the two configurations considered in this work. (a) Large-diameter InAs nanowire (pink-gray cylinder) positioned inside and parallel to the transmission line (blue-gray). The disk-shaped quantum dots (QDs) are located in the nanowire and are formed by two InP boundaries (brown-dark gray). Each QD contains only one electron with spin 1/2 (green arrows). (b) Two small-diameter InAs nanowires (pink-gray) positioned perpendicularly to the transmission line (blue-gray). The elongated QDs are oriented along the nanowire with one electron in each dot. The QD confinement can be achieved by barrier materials (as shown in brown-dark gray) or by external gates (not shown).

optical cavities in semiconductors was also the subject of some recent experiments.[32,33]

Very recently, one-dimensional (1D) electromagnetic cavities (or transmission lines) were shown to be very suitable for reaching the strong coupling regime between superconducting qubits and photons.[34–36] Theoretical extension to QDs were proposed subsequently, including charge and spin qubits.[37,38] The direct coupling of the spin to the cavity modes via the magnetic dipole transitions is usually weak, and one has to use electric-dipole transitions together with correlations between spin and charge degrees of freedom in order to obtain a sizable effective coupling. This can be achieved in several ways, e.g., by making use of the Pauli exclusion principle and Coulomb repulsion,[38] or of Raman transitions.[37]

Here, we propose another mechanism to achieve long-distance coupling between spins inside a cavity, namely, via SOI which leads to an effective coupling of spin to the electric field component of the cavity photon and thus eventually to a coupling between distant spins mediated by this photon. In order to reach a sizable coupling strength, it is desirable to use nanostructures with large SOI such as InAs QDs. Two such proposed configurations, which define the two model systems to be studied in this paper, are sketched in Figs. 1(a) and 1(b). They consist of nanowire QDs embedded in a transmission line. In particular, in Fig. 1(a), a nanowire positioned *parallel* to the transmission line axis is shown. In this case, the QDs are realized by confining the electrons in the longitudinal direction (i.e., along the nanowire axis) much stronger than in the transverse one. This corresponds to a nanowire with a large diameter, on the order of 80–100 nm. Such longitudinal confinement can be achieved by applying metallic gates or by using other materials as barriers (InP, for example, which is depicted in Fig. 1 in brown-dark gray) which have a larger band gap than the host material such as, e.g., InAs.[6,23] In Fig. 1(b), a small-diameter ($D<40$ nm) InAs nanowire is shown, being positioned perpendicularly to the transmission line and containing QDs that are elongated along the nanowire. That means, that in this case, we assume that the electronic confinement along the nanowire is much weaker than in the transverse direction. Then, to a very good approximation, the electrons can be considered as behaving one dimensionally, which will allow us to treat the SOI exactly, while this is not possible for the configuration in Fig. 1(a). However, in order to prevent a current flow, the nanowire and the transmission line need to be separated by some insulating coating material obtained, for example, by atomic layer deposition.

The goal of our work is now to analyze these configurations in detail and, in the first part of the paper, to derive an effective spin-spin coupling Hamiltonian. In the second part, we study the spin decay in this system, induced by phonons and SOI, and calculate explicitly the spin relaxation and decoherence times due to this mechanism. We will show that these times are much longer than the switching times needed to manipulate and couple the spins coherently. Thus, our findings provide theoretical evidence that nanowire QDs embedded into transmission lines are promising candidates for spin qubits with tunable long-range coupling. This scheme also opens the door to hybrid configurations where qubits of different nature (e.g., superconducting and spin qubits) can be coupled via the transmission line.

The paper is organized as follows. In Sec. II, we introduce the model for our system, namely, single-electron QDs and cavity, and specify the model Hamiltonian. In Sec. III, we derive first the effective spin-photon Hamiltonian for a single spin in the cavity for a general SOI. Here, we derive also the general effective spin-spin coupling induced by the SOI and the cavity photon modes. In Sec. IV, we investigate the case of a QD strongly confined in the longitudinal direction. Then, in Sec. V, we analyze the opposite case when the electron is strongly confined in the transverse direction of the nanowire. In Sec. VI, we provide some numerical estimates for the strengths of the spin-photon and spin-spin couplings for both cases. Then, in Sec. VII, we give a brief description of the manipulation of the spins by electric fields. In Sec. VIII we study the spin decay and provide a detailed description of the relaxation of the spin via SOI and acoustic phonons. Some technical details of the phonon analysis are deferred to the Appendix. Finally, conclusions are given in Sec. IX.

II. MODEL HAMILTONIAN

The Hamiltonian of the system composed of the single-electron QD and the cavity reads

$$H = \frac{p^2}{2m^{*}_2} + V(\boldsymbol{r}) + \frac{1}{2} g \mu_B \boldsymbol{B} \cdot \boldsymbol{\sigma} + H_{SO} + H_{e\text{-}\gamma} + H_{\gamma}, \quad (1)$$

where the first two terms represent the bare orbital part of the Hamiltonian, m^* is the effective mass of the electron, g is the g factor of the electron in the material, and $V(\boldsymbol{r})$ is the confinement potential, both in the longitudinal and transverse directions. We can obtain an effective Hamiltonian H_{eff} by averaging over the ground state $|0\rangle$ in the longitudinal or in the transverse directions depending on which case in Fig. 1 is considered. Then, for the system in Fig. 1(a) [Fig. 1(b)], we obtain an effective 2D (1D) Hamiltonian.

The third term stands for the Zeeman interaction, while the fourth term in Eq. (1) represents the SOI. For wurtzite InAs nanowires grown along the c axis, with the longitudinal confinement much stronger than the transverse one [see Fig. 1(a)], the SOI takes the form of a Rashba type,[5] $H_{SO} \equiv H^t_{SO} = \alpha(\boldsymbol{p} \times \boldsymbol{c}) \cdot \boldsymbol{\sigma}$, with $\boldsymbol{c}$ being the unit-vector corresponding to the direction of the c-axis of the crystal. This expression when written in components becomes

$$H^t_{SO} = \alpha(p_x \sigma_y - p_y \sigma_x). \quad (2)$$

We mention that our present study is quite general and can be easily adapted to other types of SOIs (such as Dresselhaus type). In the opposite case, when the transverse confinement is much stronger than the longitudinal one [see Fig. 1(b)], the SOI Hamiltonian H_{SO} takes the form $H_{SO} \equiv H^l_{SO} = (\boldsymbol{k} \cdot \boldsymbol{c})(\boldsymbol{\eta} \cdot \boldsymbol{\sigma})$ which, when written in components, becomes

$$H^l_{SO} = \eta p_x \sigma_{\boldsymbol{\eta}}, \quad (3)$$

with $\boldsymbol{\eta} = (\eta_x, \eta_y, \eta_z)$ being a vector of coupling constants and $\sigma_{\boldsymbol{\eta}}$ being the spin component along $\boldsymbol{\eta}$.[5]

The fifth term represents the interaction between the photons in the cavity, labeled γ, and the electron in the QD. This term is given by

$$H_{e\text{-}\gamma} = e\boldsymbol{E}(z) \cdot \boldsymbol{r}. \quad (4)$$

The electric field acting on the electron is given by $\boldsymbol{E}(z) = \boldsymbol{e}_x V(z)/d$, with $\boldsymbol{e}_x$ being the unit vector along x, $V(z)$ represents the fluctuating potential within the transmission line, and d is the distance between the transmission line and the center conductor. The voltage fluctuation $V(z)$ has the following form:[35]

$$V(z) = \sum_{p=1}^{\infty} V_p \sin\left(\frac{p\pi z}{L}\right)[a_p + a_p^{\dagger}], \quad (5)$$

where $V_p = \sqrt{\hbar \omega_p / Lc}$, $a_p^{\dagger}$ (a_p) are the creation (annihilation) operators for the excitations (photons), c is the capacitance per unit length, L is the length of the resonator, and ω_p is the eigenmodes of the resonator. The last term in the Hamiltonian represents the free photons $H_{\gamma} = \Sigma_p \hbar \omega_p a_p^{\dagger} a_p$.

From Eq. (1), we see that there exists an infinite number of frequencies in the transmission line, implying a coupling of the electron charge to an infinite number of modes. However, from all these modes, the relevant ones are those close to resonance with the Zeeman splitting of the spin. In the following, we disregard all other modes from the problem and we assume also that the QD is in the center of the transmission line, so that the interaction between the electron charge and the photons becomes maximal. Having now defined all the ingredients, we can proceed to study the dynamics of the system.

III. GENERAL SPIN-PHOTON DYNAMICS

A. Spin-photon interaction

In the following, we derive an effective spin-photon Hamiltonian, assuming for both cases in Fig. 1 a SOI of arbitrary strength (to be restricted later on). In the case of time-reversal symmetry, the ground state of the dot ($H_d \equiv H_0 + H_{SO} + H_Z$) is twofold degenerate (Kramers doublet), while this degeneracy is lifted in the presence of a magnetic field. If the magnetic field is such that the doublet splitting and also the electron-photon coupling strength are smaller than the level spacing of the QD, we can restrict our considerations to the dynamics of the lowest doublet only. We label this doublet by $\{|\Uparrow\rangle, |\Downarrow\rangle\}$, which is now different from the "true" electron spin. In the absence of SOI interaction, the true electron spin will not couple to electric fields by any means, while in the presence of SOI, the lowest Kramers doublet will contain orbital part to some amount, allowing coupling to electric fields (quantum or classical). Of course, the amount of orbital part contained will depend on the strength of the SOI compared, for example, to the bare orbital level spacing in the QD. It is of major importance to quantify the amount of orbital degrees of freedom contained in this Kramers doublet by taking as a reference the Kramers doublet free of SOI, i.e., the lowest bare spin state (being the direct product of orbital state and spin state). Assuming for simplicity that the SOI-free Hamiltonian has no degenerate levels (beside the Kramers doublets), we could, in principle, obtain the states in the presence of SOI (arbitrarily strong) from the ones without it by switching on the SOI adiabatically, so that we achieve a continuous mapping of states.

Assuming the above mentioned adiabatic switching on of SOI, we can connect formally the states in the presence of the SOI to the ones in the absence of it with the help of a unitary transformation or Schrieffer-Wolff (SW) transformation

$$|n_{\tau}\rangle = e^{-S}|n\rangle|\sigma\rangle, \quad (6)$$

where the states $|n\rangle$ are the eigenstates of the Hamiltonian H_0 ($H_0|n\rangle = E^0_n|n\rangle$), $|n_{\tau}\rangle$ are the Kramers doublets with SOI, $|\sigma\rangle = |\uparrow, \downarrow\rangle$ are the bare spin states, and $S = -S^{\dagger}$. Also, the relation $H_d|n_{\tau}\rangle = E^{n_{\tau}}_d|n_{\tau}\rangle$ holds from our definition of the transformed state. For notational convenience, we denote the lowest Kramers doublet as $|0_{\tau}\rangle$. This is written simply as $|0_{\tau}\rangle \equiv |\tau\rangle$, with the identification $|\tau\rangle = \{|\Uparrow\rangle, |\Downarrow\rangle\}$. The above transformation can be performed on the level of the Hamiltonian, implying diagonalization of the Hamiltonian H_d in the basis of the "bare" Hamiltonian H_0,

$$\bar{H} \equiv e^{-S} H e^{S}. \tag{7}$$

The advantage of transforming the Hamiltonian H_d so that it becomes diagonal in the basis of the bare Hamiltonian H_0 is now obvious. Within this transformation, one can, in principle, proceed to calculate the effect of SOI to arbitrary order in perturbation theory, together with the SOI-induced spin-photon coupling. We can now derive an effective spin-photon Hamiltonian within the lowest doublet $|\tau\rangle$ by averaging $\bar{H}$ over the orbital ground state $|0\rangle$. This leaves us with the following effective spin-photon Hamiltonian $H_{s\text{-}\gamma} \equiv \langle 0|\bar{H}|0\rangle$ given by

$$H_{s\text{-}\gamma} = \frac{1}{2} g \mu_B B_{eff} \sigma_z + \boldsymbol{\mathcal{M}}_\gamma \cdot \boldsymbol{\sigma}(a^\dagger + a) + \hbar \omega a^\dagger a, \tag{8}$$

where

$$\frac{1}{2} g \mu_B B_{eff} \sigma_z = \langle 0|e^{-S} H_d e^{S}|0\rangle \tag{9}$$

stands for the renormalized magnetic field and

$$\boldsymbol{\mathcal{M}}_\gamma \cdot \boldsymbol{\sigma} = \frac{eV_1}{d} \langle 0|e^{-S} y e^{S}|0\rangle \tag{10}$$

stands for the spin-photon coupling. Above, we also introduced the simplified notations $\omega_1 \equiv \omega$ and $a_1^\dagger \equiv a^\dagger$ $(a_1 \equiv a)$. We mention that in order to have a finite coupling of the spin $\boldsymbol{\sigma}$ to the photons, the vector $\boldsymbol{\mathcal{M}}_\gamma$ must contain some time-reversal breaking parameter, such as the external magnetic field B. In the absence of the magnetic field, there is no coupling between the lowest doublet and the photons $(\boldsymbol{\mathcal{M}}_\gamma = 0)$ to all orders in SOI.

We now define the spin-photon coupling strength $\nu = \sqrt{(\mathcal{M}_\gamma^x)^2 + (\mathcal{M}_\gamma^y)^2}$ and the detuning of the qubit from the cavity by $\Delta \equiv E_Z^{eff} - \hbar\omega$, where $E_Z^{eff} \equiv g\mu_B B_{eff}$. Close to the resonance between the qubit and the cavity mode $(\Delta \ll E_Z^{eff}, \hbar\omega)$, one can simplify Eq. (8) by using the so-called rotating wave approximation (RWA).[39] This implies to switch first to the interaction picture, so that the operators $a(a^\dagger)$ and $\sigma_\mp$, where $\sigma_\mp = \sigma_x \mp i\sigma_y$, become time dependent,

$$\sigma_\mp(t) = \sigma_\mp(0) e^{\mp i \omega_Z^{eff} t}, \tag{11}$$

$$a(t) = a(0) e^{-i\omega t}, \tag{12}$$

$$\sigma_z(t) = \sigma_z(0). \tag{13}$$

where $\omega_Z^{eff} = E_Z^{eff}/\hbar$. Then, we neglect the terms in the time-dependent resulting Hamiltonian, which oscillate fast on the time scale $\hbar/\Delta$. This means neglecting counter-rotating terms such as $a^\dagger \sigma_+ \sim e^{i(\omega_Z^{eff} + \omega)t}$, $a\sigma_- \sim e^{-i(\omega_Z^{eff} + \omega)t}$, $a^\dagger \sigma_z \sim e^{i\omega t}$, and $a\sigma_z \sim e^{-i\omega t}$, which average to zero for large times. Within this approximation, the Hamiltonian in Eq. (8) within the interaction picture becomes static and of the form

$$H_{s\text{-}\gamma}^{eff} = \frac{1}{2} g \mu_B B_{eff} \sigma_z + \nu(a^\dagger \sigma_- + \sigma_+ a) + \hbar\omega a^\dagger a. \tag{14}$$

As expected, the above expression agrees with the Jaynes-Cummings Hamiltonian.[40]

B. Effective spin-spin interaction

We now investigate the case of two QDs in the cavity in the limit of finite detunings $\Delta_{1,2}$. The Hamiltonian $H_{s\text{-}\gamma}^{(2)}$ corresponding to the two spins in the cavity can be found by just extending Eq. (14) to two spins,

$$H_{s\text{-}\gamma}^{(2)} = \sum_{i=1,2} \left(\frac{1}{2} g_i \mu_B B_{eff}^i \sigma_z^i + \nu_i (a^\dagger \sigma_-^i + \sigma_+^i a) \right) + \hbar\omega a^\dagger a. \tag{15}$$

For $\nu_i/\Delta_i \ll 1 (i = 1,2)$, the spin-photon interaction can be treated within the second order perturbation theory in ν_i. We use again the SW transformation, similar to the previous section. Here, this implies finding an operator T so that

$$\tilde{H}_{s\text{-}\gamma}^{(2)} = e^T H_{s\text{-}\gamma}^{(2)} e^{-T} \tag{16}$$

is diagonal in the basis of the spin-photon Hamiltonian without spin-photon interaction (the Hamiltonian $H_{s\text{-}\gamma}^{(2)}$ with $\nu_{1,2} \equiv 0$). Within first order in spin-photon couplings $\nu_{1,2}$, the transformation operator T reads

$$T = \sum_{i=1,2} \frac{\nu_i}{\Delta_i} (\sigma_+^i a - a^\dagger \sigma_-^i), \tag{17}$$

under the assumption that the condition $\nu_i/\Delta_i \ll 1$, $i = 1,2$, is satisfied for both dots. The transformed Hamiltonian $\tilde{H}_{s\text{-}\gamma}^{(2)}$ becomes

$$\tilde{H}_{s\text{-}\gamma}^{(2)} = \left(\hbar\omega + \frac{2\nu_1^2}{\Delta_1} \sigma_z^1 + \frac{2\nu_2^2}{\Delta_2} \sigma_z^2 \right) a^\dagger a + \left(E_{1Z}^{eff} + \frac{\nu_1^2}{\Delta_1} \right) \sigma_z^1 + \left(E_{2Z}^{eff} + \frac{\nu_2^2}{\Delta_2} \right) \sigma_z^2 + \nu_1 \nu_2 \left(\frac{1}{\Delta_1} + \frac{1}{\Delta_2} \right) (\sigma_+^1 \sigma_-^2 + \sigma_+^2 \sigma_-^1), \tag{18}$$

where $E_{iZ}^{eff} = g\mu_B B_{eff}^i$. We can obtain a pure spin Hamiltonian by neglecting the fluctuations of the photon number $a^\dagger a \to \langle a^\dagger a \rangle \equiv \bar{n}$, with $\bar{n}$ the average number of photons in the lowest cavity mode. The resulting Hamiltonian $H_s \equiv \tilde{H}_{s\text{-}\gamma}^{(2)}|_{a^\dagger a \to \bar{n}}$ reads

$$H_s = \tilde{E}_Z^1 \sigma_z^1 + \tilde{E}_Z^2 \sigma_z^2 + J(\sigma_+^1 \sigma_-^2 + \sigma_+^2 \sigma_-^1), \tag{19}$$

where

$$\tilde{E}_Z^i = E_{iZ}^{eff} + 2\left(\bar{n} + \frac{1}{2} \right) \frac{\nu_i^2}{\Delta_i}, \quad i = 1,2, \tag{20}$$

$$J = \nu_1 \nu_2 \left(\frac{1}{\Delta_1} + \frac{1}{\Delta_2} \right). \tag{21}$$

In Eq. (20), we see that the effective Zeeman splitting $\tilde{E}_Z^i$ is quite different from the bare one, $E_{iZ} \equiv g_i \mu_B B$. Besides the

SOI renormalization of the Zeeman splitting, there is also a contribution from the spin-photon coupling, which consists of the Lamb shift (the term independent of the average photon number $\bar{n}$) and the ac Stark shift (the term proportional to the average photon number $\bar{n}$).

The expression in Eq. (19) is one of our main results: In the presence of SOI and cavity modes, one can achieve an effective spin-spin coupling with the exchange coupling J between two spins that are spatially well separated. Indeed, this interaction can act over the entire length of the cavity, which can be as large as a few millimeters. Also, the spin-spin interaction is of XY type (transverse spin-spin coupling), which, together with single-spin rotations, has been shown to be universal for quantum computing.[31,41] We mention that in order to obtain a maximal effect, one should be able to tune the two qubits into resonance, so that $\tilde{E}_Z^1 = \tilde{E}_Z^2$.[31]

IV. STRONG LONGITUDINAL CONFINEMENT

So far, we have taken the SOI into account exactly, regardless of the system under consideration, but under the assumption that the lowest Kramers doublet is well separated from the higher states compared to Zeeman energy and electron-photon coupling. We analyze here the spin-photon coupling for the case shown in Fig. 1(a). As stated in Sec. II, in this case, we can derive an effective transverse Hamiltonian $H_{eff} \equiv H_t = \langle 0_l | H | 0_l \rangle$, where $|0_l\rangle$ stands for the ground-state wave function in the longitudinal direction z. The effective Hamiltonian H_t reads

$$H_t = \frac{p_x^2 + p_y^2}{2m^*} + V(x,y) + H_Z + H_{SO}^t + H_{e\text{-}\gamma} + H_\gamma, \tag{22}$$

with $V(x,y) = \langle 0_l | V(\boldsymbol{r}) | 0_l \rangle$, while all the other terms stay the same since they do not act in the z direction. In the above expression, we disregarded the term $\langle 0_l | (p_z^2/2m^*) | 0_l \rangle$, as it gives a constant shift of the levels.

We can start, in principle, to derive the spin-photon interaction from the effective Hamiltonian H_t by making use of transformation (6). However, this cannot be done exactly, and we have to proceed in perturbation theory. In order to give some numerical estimates for the strength of the coupling ν, we assume the limit of weak SOI, quantified by the condition $R/\lambda_{SO} \ll 1$, with R being the dot (wire) radius and $\lambda_{SO} = \hbar/m^*\alpha$ the spin-orbit length.[29,42,43] Then, we can treat the SOI in perturbation theory. We assume in the following hard-wall boundary conditions for the electrons confined in the QDs, namely, circular hard-wall boundaries in the transverse direction. In the longitudinal direction, the electron is also confined by a hard-wall type of potential, but much stronger than in the transverse direction, as stated before. We compute the operator S from Eq. (6) within the first order in SOI, $S \approx (L_0 + L_Z)^{-1} H_{SO}$, which gives explicitly

$$S \approx i\boldsymbol{\xi} \cdot \boldsymbol{\sigma} - E_Z L_0^{-1} (\boldsymbol{b} \times \boldsymbol{\xi}) \cdot \boldsymbol{\sigma}, \tag{23}$$

in the limit of $E_Z \ll \Delta E_0$ with $\Delta E_0 = E_1 - E_0$ being the energy difference between the first excited state $|1\rangle$ and the ground state $|0\rangle$ in the QD. In the above formulas, the Liouvilleans $L_{0,Z}$ are defined as $L_{0,Z}A = [H_{0,Z}, A], \forall A$ and $\boldsymbol{\xi} = \lambda_{SO}^{-1}(-y, x, 0)$, $\boldsymbol{b} = \boldsymbol{B}/B$. We can obtain an effective Hamiltonian up to second order in SOI and first order in Zeeman splitting for the lowest Kramers doublet by averaging over the orbital ground state $|0\rangle$,

$$H_{s\text{-}\gamma} = \frac{1}{2} g \mu_B \boldsymbol{B} \cdot \boldsymbol{\sigma} + \langle 0 | [S, H_{SO}] | 0 \rangle + \langle 0 | [S, H_{e\text{-}\gamma}] | 0 \rangle + \frac{1}{2} \langle 0 | [S, [S, H_{e\text{-}\gamma}]] | 0 \rangle + H_\gamma. \tag{24}$$

The orbital wave functions have the form (for circular hard-wall boundary conditions)

$$\psi_{mp}(r) = \frac{1}{\sqrt{\pi} R} \frac{e^{im\phi}}{J_{|m|+1}(k_{mp}R)} J_{|m|}(k_{mp} r), \tag{25}$$

where $J_{|m|}(k_{mp}r)$ are the Bessel functions of the first kind, r is the electron radial coordinate in the transverse direction, and k_{mp} are the solutions of the equation $J_{|m|}(k_{mp}R) = 0$. The appropriate energies are given by $E_{mp} = \hbar^2 k_{mp}^2 / 2m^*$. Also, we assume that the magnetic field $\boldsymbol{B}$ and the fluctuating electric field $\boldsymbol{E}$ are both pointing along the x direction, such that $H_{e\text{-}\gamma} = eEx$ and $S = i\boldsymbol{\xi} \cdot \boldsymbol{\sigma} - (E_Z/\lambda_{SO}) L_0^{-1} x \sigma_z$. After performing the integrations, we are left with the following effective Hamiltonian:

$$H_{s\text{-}\gamma} = \frac{1}{2} E_Z^{eff} \sigma_z + \mathcal{M}_\gamma^x (a^\dagger + a) \sigma_y + H_\gamma, \tag{26}$$

with

$$E_Z^{eff} \simeq E_Z \left(1 - 0.25 \left(\frac{R}{\lambda_{SO}} \right)^2 \right), \tag{27}$$

$$\mathcal{M}_\gamma^x \simeq 0.25 eER \frac{E_Z}{\Delta E_0} \frac{R}{\lambda_{SO}}. \tag{28}$$

We see that there is no second order contribution in SOI to the spin-photon interaction, this contribution vanishes identically for cylindrical wires in the ground state. We mention that within the RWA, the Jaynes-Cummings coupling ν becomes $\nu = \mathcal{M}_\gamma^x$.

In the case of two spins present in the cavity, one obtains the same expression as in Eq. (19), where $\nu_{1,2}$ is given by Eq. (28). Since our coupling is proportional to the bare Zeeman splitting E_Z, we need large magnetic fields in order to obtain a sizable coupling. Then, we can, in principle, neglect the Lamb and the ac Stark shifts in the expressions for $\tilde{E}_Z^i$, since they give negligible renormalizations, so that $\tilde{E}_Z^i \approx E_{iZ}^{eff}$. However, as can be seen from Eq. (27), the Zeeman splitting can be strongly reduced for large SOI. This feature will turn out to be very important in order to have a long-lived qubit (see below).

V. STRONG TRANSVERSE CONFINEMENT

In this section, we analyze the case shown in Fig. 1(b), i.e., when the transverse confinement in the y-z plane is much stronger than the longitudinal one along $\hat{x}$. As in the

previous case, we can derive an effective longitudinal Hamiltonian by averaging the full Hamiltonian H over the transverse orbital ground state $|0_t\rangle$. The effective Hamiltonian $H_{eff} \equiv H_l = \langle 0_t|H|0_t\rangle$ reads

$$H_l = \frac{p_x^2}{2m^*} + V(x) + H_Z + H_{SO}^l + H_{e\text{-}\gamma} + H_\gamma, \tag{29}$$

with $V(x) = \langle 0_t|V(\boldsymbol{r})|0_t\rangle$, while all other terms remain the same, since they have no action along the x direction. Again, like in the previous case, we disregard the term $\langle 0_t|(p_y^2 + p_z^2)/2m^*|0_t\rangle$, since it gives a constant shift of the levels.

We now derive the spin-photon interaction from the effective Hamiltonian (29). As can be seen from Eq. (3), the SOI contains only one spin component, $\sigma_{\boldsymbol{\eta}}$ along the $\boldsymbol{\eta}$ direction. In this case and in the absence of an external magnetic field, the SW transformation (6) can be performed exactly, since the SOI appears as an Abelian gauge potential.[44,45] In the presence of an external magnetic field, however, this cannot be done exactly anymore. We now apply transformation (6) to the Hamiltonian H_l so that we obtain $\bar{H}_l = e^{-S} H e^S$, with the operator S corresponding to the zero-field case. This operator S reads

$$S = -i\frac{x}{\lambda_{SO}}\sigma_{\boldsymbol{\eta}}, \tag{30}$$

with $\lambda_{SO} = \hbar/m^*\eta$. The effect of this transformation can be evaluated exactly, and we obtain

$$\bar{H}_l = \frac{p_x^2}{2m^*} + V(x) + H_Z(x) + eEx + \hbar\omega a^\dagger a, \tag{31}$$

with

$$H_Z(x) = \frac{1}{2}g\mu_B\left(\cos\left(\frac{2x}{\lambda_{SO}}\right)\boldsymbol{B}_{\boldsymbol{\eta}\perp}\cdot\boldsymbol{\sigma} + B_{\boldsymbol{\eta}}\sigma_{\boldsymbol{\eta}} - \sin\left(\frac{2x}{\lambda_{SO}}\right)(\boldsymbol{e}_{\boldsymbol{\eta}}\times\boldsymbol{B})\cdot\boldsymbol{\sigma}\right), \tag{32}$$

where $\boldsymbol{B}_{\boldsymbol{\eta}\perp}$ is the component of the magnetic field $\boldsymbol{B}$ perpendicular to the vector $\boldsymbol{\eta}$, $B_{\boldsymbol{\eta}}$ is the magnetic field component along $\boldsymbol{\eta}$, and $\boldsymbol{e}_{\boldsymbol{\eta}} = \boldsymbol{\eta}/\eta$. We now assume, as before, that the Zeeman splitting $E_Z = g\mu_B B$ is much smaller than the orbital level spacing ΔE_0 given by the first two terms in the above Hamiltonian. Also, we assume harmonic confinement potential along the x direction, $V(x) = m^*\omega_0^2 x^2/2$, which gives a dot size $l = \sqrt{\hbar/m^*\omega_0}$. This is usually the case for gate-defined QDs. Then, the above condition translates in having $E_Z \ll \hbar\omega_0$. We are now in the position to derive an effective spin-photon Hamiltonian by treating $H_Z(x)$ in perturbation theory. We perform a new SW transformation and transform the above Hamiltonian into a diagonal one in the basis of H_0 to obtain $H_{s\text{-}\gamma} = \langle 0|e^{-S'}\bar{H}e^{S'}|0\rangle$. We averaged also over the orbital ground state $|0\rangle$ to obtain a pure spin-photon Hamiltonian. Within lowest order in $E_Z/\hbar\omega_0$, the transformation is given by $S' = (1-\mathcal{P})L_0^{-1}H_Z(x)$. After inserting the operator S' in the expression for $H_{s\text{-}\gamma}$ and keeping only the lowest order corrections, we obtain

$$H_{s\text{-}\gamma} = \frac{1}{2}g\mu_B\boldsymbol{B}_{eff}\cdot\boldsymbol{\sigma} + \boldsymbol{\mathcal{M}}_\gamma\cdot\boldsymbol{\sigma}(a^\dagger + a) + \hbar\omega a^\dagger a, \tag{33}$$

with

$$\boldsymbol{B}_{eff}\cdot\boldsymbol{\sigma} = e^{-(l/\lambda_{SO})^2}\boldsymbol{B}_{\boldsymbol{\eta}\perp}\cdot\boldsymbol{\sigma} + B_{\boldsymbol{\eta}}\sigma_{\boldsymbol{\eta}}, \tag{34}$$

$$\boldsymbol{\mathcal{M}}_\gamma\cdot\boldsymbol{\sigma} = eV_1\frac{l}{d}\frac{l}{\lambda_{SO}}\frac{E_Z}{\hbar\omega_0}e^{-(l/\lambda_{SO})^2}(\boldsymbol{e}_{\boldsymbol{\eta}}\times\boldsymbol{b})\cdot\boldsymbol{\sigma}. \tag{35}$$

We see that the spin-photon interaction is maximal when the magnetic field is perpendicular to $\boldsymbol{\eta}$, like in the perturbative calculation of the previous section. This is expected since, as in the previous section, the SOI manifests itself as an Abelian gauge potential in lowest order, although there are two spin components. For the rest of the paper, we assume now a magnetic field perpendicular to $\boldsymbol{\eta}$ so that $B_{\boldsymbol{\eta}} = 0$, $\boldsymbol{B}\cdot\boldsymbol{\sigma}_{\boldsymbol{\eta}\perp} = B\sigma_{\tilde{z}}$ and $(\boldsymbol{e}_{\boldsymbol{\eta}}\times\boldsymbol{b})\cdot\boldsymbol{\sigma} = \sigma_{\boldsymbol{\eta}\perp,\boldsymbol{b}} \equiv \sigma_{\tilde{x}}$. Then, the spin-photon Hamiltonian reads

$$H_{s\text{-}\gamma} = \frac{1}{2}E_Z^{eff}\sigma_{\tilde{z}} + \mathcal{M}_\gamma\sigma_{\tilde{x}}(a^\dagger + a) + \hbar\omega a^\dagger a, \tag{36}$$

with

$$\mathcal{M}_\gamma = eV_1\frac{l}{d}\frac{l}{\lambda_{SO}}\frac{E_Z^{eff}}{\hbar\omega_0}, \tag{37}$$

where $E_Z^{eff} = E_Z e^{-(l/\lambda_{SO})^2}$ is the effective Zeeman splitting.

We see that the SOI reduces strongly the Zeeman splitting for large values of the ratio l/λ_{SO}. This overscreening of the Zeeman interaction can be understood as follows. After performing transformation (30), there is no SOI present in the system, but the magnetic field in the new "frame" has an oscillatory behavior, as shown in Eq. (32). This means that the magnetic field precesses around the x direction, the speed of precession being given by the strength of the SOI measured through the SO length λ_{SO}. If the bare Zeeman splitting E_Z is much smaller that the orbital level spacing, $E_Z \ll \hbar\omega_0$, the electron find itself in the orbital ground state $|0\rangle$ given by H_0. Then, if the SOI strength is increased, the precession frequency increases also, so that there are many precessions of the magnetic field over small distances. Since this implies also small changes of the orbital wave function, this leads to an average reduction of the effective Zeeman splitting, as obtained above.

VI. NUMERICAL ESTIMATES

We give now some estimates for the coupling $\nu \equiv \mathcal{M}_\gamma^x$ for QDs in InAs nanowires for both geometries shown in Fig. 1. In the first case, we assume the dots to have a width of 5–10 nm ($E_w \approx 10$ meV—the transverse confining energy) and a radius $R \approx 50$ nm ($\Delta E_0 \approx 5$ meV). The electron in the QD is characterized by $m^* = 0.023 m_e$, $g \approx 2.5$, and $\lambda_{SO} \approx 100$ nm.[5] We assume also that the 1D cavity is 2 mm long and 100 nm wide, $c \approx 2\times 10^{-10}$ C/V m,[35] which implies for the fundamental mode $\hbar\omega \simeq 0.5$ meV and an rms electric field $E = V_1/d \simeq 100$ V/m. The Zeeman splitting is assumed to be of the same order of magnitude as the energy of the

lowest cavity mode, i.e., $E_Z^{eff} \approx 0.5$ meV ($B \approx 1.75$ T). Plugging in all the numbers in the formula for ν, Eq. (28), we obtain $\nu \approx 10^{-5}$ meV which, in the degenerate case $E_Z^{eff} = \hbar\omega$, corresponds to a dynamics of the spin-photon system of about 60 ns (Rabi oscillations between the spin and the cavity). In the second case, there is more control on the orbital level spacing since the dots are obtained, in principle, by external gating. We now assume a dot radius $R \approx 10$ nm ($E_{0t} \simeq 30$ meV), a dot length $l \simeq 40$ nm ($\hbar\omega_0 \simeq 2$ meV), and $g \approx 10$.[6] For $E_Z^{eff} \approx 0.5$ meV, we need a magnetic field $B \approx 0.45$ T. Also, we assume the same lengths for the cavity as for the first case so that we obtain $\nu \approx 4 \times 10^{-4}$ meV. This gives rise to a dynamics of the spin-photon system of about 2 ns in the degenerate limit $E_Z^{eff} = \hbar\omega$. We mention that in both cases, the renormalized Zeeman splitting is quite different from the bare one, i.e., $E_Z^{eff} = 0.93 E_Z$ in the first case and $E_Z^{eff} = 0.84 E_Z$ in the second case.

For the exchange coupling J between two spins, one can achieve values as large as $J \approx 10^{-6}$ meV in the limit of quite small detunings ($\Delta \approx 10^{-4}$ meV) for the case in Fig. 1(a), which eventually translates into a time dynamics of about 500 ns for coherently swapping the two spins. In the geometry shown in Fig. 1(b), the exchange coupling J can be much larger, on the order of $J \approx 4 \times 10^{-5}$ meV for detunings on the order of $\Delta \approx 4 \times 10^{-3}$ meV, which implies a time dynamics of about 20 ns for swapping the two spins coherently.

In order to control the exchange coupling J, one should be able, in principle, to change the Zeeman splitting or the orbital level spacing. In InAs QDs, the Zeeman splitting can be changed very efficiently by changing the dot size along the wire direction,[6] in both cases in Fig. 1. Considering the case of two QDs in the cavity, one way to decouple them is by tuning the g factors so that $\Delta_1 = -\Delta_2$, as can be seen from Eq. (18). However, in the case of many QDs inside the cavity, this will be rather difficult to achieve.

Another possibility is to change the g factors locally so that the coupling between the spins reduces due to the reduction of the Zeeman splitting E_Z. Assuming that a reduction of J by 1 order of magnitude is a good measure for the decoupling, one obtains a corresponding change in the g factor of the order of 15% in the first geometry shown in Fig. 1. The rather drastic change of g factor was already experimentally demonstrated for InAs QDs by Björk *et al.*[6] They achieved a change in the g factor from $|g| = 3.5$ to $|g| = 2.3$ when the dot size along the nanowire was reduced from 10 to 8 nm, i.e., a variation of about 30%, which shows to be sufficient for our scheme in the geometry shown in Fig. 1. The same can be done efficiently for the second geometry, since the dots being gate defined can be modified strongly along the wire axis.

Yet another way to change the exchange coupling J is by changing the orbital confining energy ΔE_0. In the first geometry $\nu \sim R^4$, and $J \sim \nu^2$ (assuming two equal spin-photon couplings for simplicity), one obtains a dependence $J \sim R^8$. Then, by using top gates, for example, one can strongly modify the exchange coupling J by a small change of the orbital energy ΔE_0. This can be done equally, and maybe more efficiently, for the second geometry since, as explained above, the dots can be modified easily along the wire axis. The spin-photon coupling $\nu \sim l^4$, which implies then a scaling of the exchange coupling $J \sim l^8$.

VII. COHERENT MANIPULATION

One way to coherently manipulate and to read out (measurement) the qubits is by applying an external driving field to the cavity with a varying frequency $H_{ex} = \epsilon(t)(a^\dagger e^{-i\omega_{ex}t} + a e^{i\omega_{ex}t})$, where $\epsilon(t)$ is the amplitude. In the dispersive limit ($\nu_i/\Delta_i \ll 1$), $H_{ex} \to H_{ex} + [T, H_{ex}]$, so that

$$H_{ex} \simeq \epsilon(t) a^\dagger e^{-i\omega_{ex}t} + \sum_{i=1,2} \frac{\nu_i \epsilon(t)}{\Delta_i} \sigma_i^+ e^{-i\omega_{ex}t} + \text{H.c.} \quad (38)$$

The control of the ith qubit can now be realized by tuning the frequency of the driving field to $\omega_{ex} = E_{iZ}^{eff} + \nu_i^2/\Delta_i$, while this condition is not satisfied for the other qubits. This gives rise to an electric-dipole spin resonance (EDSR) for the ith qubit, similar to that studied by Golovach *et al.*[20] The measurement can be performed by tuning the frequency of the driving close to the cavity mode so that we can observe peaks in transmission at the positions $\hbar\omega + \Sigma_i (\nu_i^2/\Delta_i)\sigma_z^i$. If detunings are chosen so that all combinations can be distinguished, one can measure all the spins from one shot (or at least group of spins).[35]

A more efficient way to manipulate the spin is to make use of the EDSR-scheme proposed in Ref. 20, namely, to apply an alternating electric field $\mathcal{E}(t)$ to the QD, which, via the electric-dipole transitions and the SOI, gives rise to an effective alternating magnetic field. Briefly, if only the dipolar coupling to the alternating electric field $\mathcal{E}(t)$ is considered, we get $H_{e\text{-}el}(t) = e\mathcal{E}(t)y$, with the electric field $\mathcal{E}(t)$ along y-direction. If the system in Fig. 1(a) is considered, the effective spin-electric field coupling within first order in SOI becomes $H_{s\text{-}el} = \langle 0|[S, H_{e\text{-}el}(t)]|0\rangle \equiv \delta B(t)\sigma_y$, with the fluctuating magnetic field $\delta B(t)$ having the form

$$\delta B(t) \sim e\mathcal{E}(t) R \frac{E_Z}{\Delta E_0} \frac{R}{\lambda_{SO}}. \quad (39)$$

For the case shown in Fig. 1(b), we obtain a similar expression for $\delta B(t)$, but with the bare Zeeman splitting E_Z substituted with the effective Zeeman splitting E_Z^{eff} defined after Eq. (37) and the radius R substituted with the dot length l. The electric field $\mathcal{E}(t)$ is assumed to have an oscillatory behavior, $\mathcal{E}(t) = \mathcal{E}_0 \cos \omega_{ac} t$, with ω_{ac} being the frequency of the ac electric field. By tuning the frequency of the oscillatory electric field ω_{ac} in resonance with the qubit splitting E_Z^{eff}, one can achieve arbitrary rotations of the spin on the Bloch sphere on time scales given by the Rabi frequency $\omega_R = \delta B(0)/\hbar$.[20] We mention that in lowest order in SOI, the induced fluctuating magnetic field $\delta \boldsymbol{B}(t)$ is always perpendicular to the applied field $\boldsymbol{B}$ and reaches the maximum when the applied electric field $\boldsymbol{\mathcal{E}}(t)$ points into the same direction as $\boldsymbol{B}$.[20] This is the reason for choosing the electric field along the y-direction.

We give here also some estimates for the Rabi frequency ω_R. For this, we assume the same parameters as in the previous section, and we choose for the amplitude of the electric field $\mathcal{E}_0 \approx 10 \text{eV/cm}$. With this values, we obtain for the strength of the Rabi frequency $\omega_R \approx 10$ GHz, which gives a time dynamics for the electron spin control on the order of $\omega_R^{-1} \approx 0.1$ ns. This time scale must be much shorter than the

usual relaxation and decoherence times for the spin in the QD. Finding the relaxation and decoherence time scales is the subject of the next section.

VIII. SPIN RELAXATION AND DECOHERENCE

We address now the issue of relaxation and decoherence of the spin in the cavity. There are two types of contributions to the relaxation processes, one arising from the finite decay rate of the cavity, κ, and the other one from the intrinsic relaxation and decoherence of the spin, labeled by $T_{1,2}^{-1}$. To reach the strong coupling regime described here, the losses must be smaller than the coupling between the qubits J in the regime of interest ($\nu^2/\Delta > \kappa, T_{1,2}^{-1}$). Very high-$Q$ factor 1D electromagnetic cavities were already built ($Q=\kappa^{-1} \sim 10^4-10^6$),[34] so that the intrinsic relaxation and decoherence of the qubit show up as the limiting factors for reaching the strong coupling regime.

The relaxation and decoherence of the spin qubit arise mainly from the coupling to the bath of phonons and the collection of nuclei in the QD. The phonon contribution was studied microscopically in great detail for the case of gate-defined GaAs QDs in 2DEGs and it was shown that for large B fields; similar to the present case, the main contribution to relaxation comes from the deformation-potential phonons with a decay time $T_1 \sim 10^{-2}-10^{-4}$ s.[43] As a consequence, a smaller relaxation time is then expected for InAs QDs since the SOI is one order of magnitude larger than in GaAs [$T_1 \propto (\lambda_{SO}/R)^2$]. However, different from the bulk case, the phonon spectrum in nanowires becomes highly nontrivial due to the mixing of the branches by the boundaries,[46] leading to a strong modification of the relaxation time.

In cylindrical nanowires, there are three types of acoustic modes: torsional, dilatational, and flexural.[47] All these modes couple to the electric charge and, in principle, all of them couple also to the spin for a general SOI Hamiltonian. However, as shown later, this is not actually the case for the SOI acting in the two configurations in Fig. 1, and only a small part of the entire spectrum gives rise to spin relaxation.

As stated above, within the large Zeeman splitting limit considered in this paper, we can take into account only the interaction of the electron with the lattice via the deformation potential. The electron-phonon deformation-potential interaction is given by $H_{e\text{-}ph}=\Xi_0 \nabla \boldsymbol{u}(\boldsymbol{r},t)$, where Ξ_0 is the deformation-potential strength and

$$\boldsymbol{u}(\boldsymbol{r},t) = \frac{1}{\sqrt{N}} \sum_{\boldsymbol{k}} [\boldsymbol{u}(\boldsymbol{k},\boldsymbol{r}) b_{\boldsymbol{k}}(t) + \text{H.c.}], \tag{40}$$

with the displacement field $\boldsymbol{u}(\boldsymbol{k},\boldsymbol{r})$ given by[46,47]

$$\boldsymbol{u}(\boldsymbol{k},\boldsymbol{r}) = \nabla \Phi_0 + (\nabla \times \boldsymbol{e}_z)\Phi_1 + (\nabla \times \nabla \times \boldsymbol{e}_z)\Phi_2. \tag{41}$$

The index $\boldsymbol{k} \equiv \{q,n,s\}$ quantifies the relevant quantum numbers, i.e., the wave vector along the wire, the winding number, and the radial number, respectively, $b_{\boldsymbol{k}}(t)$ is the annihilation operator for phonons, $\boldsymbol{e}_z$ is the unit vector along the z direction, and

$$\Phi_j = \chi_j f_{ns}^j(r) e^{i(n\phi+qz)}, \tag{42}$$

with $j=0,1,2$, $n=0, \pm 1, \pm 2 \ldots$. The functions $f_{ns}^j(r)$ depend only on the radius,[46,48] and χ_j are normalization factors.

The effective spin-phonon interaction can be found following the same procedure as that used for deriving the spin-photon interaction for both cases in Fig. 1.

A. Spin relaxation in strongly longitudinal confined quantum dots

We give here the main steps in the derivation of the relaxation rate for the case shown in Fig. 1(a). Keeping only terms up to first order in SOI, we obtain

$$H_{s\text{-}ph} = \langle 0|[S, H_{e\text{-}ph}]|0\rangle, \tag{43}$$

with S given in Eq. (23) and $|0\rangle$ being the orbital ground state. Due to the circular symmetry, the first order in SOI term couples only to the $n=1$ phonons. The resulting spin-phonon coupling has the form

$$H_{s\text{-}ph} = \frac{1}{2} g \mu_B \delta B_y(t) \sigma_y, \tag{44}$$

with

$$\delta B_y(t) = B \frac{\Xi_0}{\Delta E_0} \frac{R}{\lambda_{SO}} \sum_{q,s} \frac{\mathcal{C}(q,s)}{\sqrt{\mathcal{F}(q,s)\rho_c \omega_{q,s}/\hbar}} K_{q,s}^2 b_{\boldsymbol{k}}^\dagger + \text{H.c.}, \tag{45}$$

$$\mathcal{C}(q,s) \approx 0.25 \int_0^1 \frac{dr r J_1(k_{11}r) J_0(k_{10}r) f_{1s}^0(r)}{|J_2(k_{11}) J_1(k_{10})|}, \tag{46}$$

where $K_{q,s}=\omega_{q,s}/c_l$ with $\omega_{q,s}$ being the eigenmodes of the phonon field and c_l the longitudinal speed of sound in InAs. The normalization function $\mathcal{F}(q,s)$ is given by

$$\mathcal{F}(q,s) = \frac{\hbar R^2}{4M\chi_0^2 \omega_{\boldsymbol{k}}}, \tag{47}$$

where M is the mass of the ions in a unit cell.

The explicit forms for the $\omega_{q,s}$ and $\mathcal{F}(\omega_{q,s})$ depend on the boundary conditions used for the phonon field. The two quantities relevant for the boundary conditions are the displacement vector $\boldsymbol{u}(\boldsymbol{r})$ and the stress vector $\boldsymbol{t}(r)=T\boldsymbol{e}_r$ at $r=R$, with T being the stress tensor[47] and $\boldsymbol{e}_r$ being the unit vector along r. One can now write $\boldsymbol{u}(\boldsymbol{r})=\mathcal{U}\boldsymbol{\chi}$ and $\boldsymbol{t}(\boldsymbol{r})=\mathcal{T}\boldsymbol{\chi}$ with $\boldsymbol{\chi}=(\chi_0,\chi_1,\chi_2)$, where the expressions for the matrices $\mathcal{U}$ and $\mathcal{T}$ are given in the Appendix. There are two limiting cases for the boundaries. The first case is met when there is zero stress at the surface, i.e., $\boldsymbol{t}(R)=0$,[47] with $\omega_{q,s}$ being the solutions of $|\mathcal{T}(R)|=0$ [free surface boundary conditions (FSBCs)], while the second limiting case is met when the surface is rigid, i.e., $\boldsymbol{u}(R)=0$, with $\omega_{q,s}$ being the solutions of $|\mathcal{U}(R)|=0$ [clamped surface boundary conditions (CSBCs)]. The phonon field is normalized according to the following relation:[49]

$$\frac{1}{\pi R^2}\int_0^{2\pi} d\phi \int_0^R dr r \boldsymbol{u}^*(\boldsymbol{k},r,\phi)\cdot\boldsymbol{u}(\boldsymbol{k},r,\phi) = \frac{\hbar}{2M\omega_{\boldsymbol{k}}}. \quad (48)$$

From the FSBCs or CSBCs, together with the normalization of the phonon field, one obtains the spectrum $\omega_{q,s}$ and the normalization function $\mathcal{F}(q,s)$.

We now use the effective spin-phonon Hamiltonian with the fluctuating field given in Eq. (44) to find the spin relaxation and decoherence times, T_1 and T_2, respectively. We mention here that the fluctuating magnetic field $\delta B_y(t)$ is perpendicular to the external one $\boldsymbol{B}$ such that there is no pure dephasing coming from the interaction of the spin with phonons in lowest order in SOI. In fact, as shown previously,[43] this is valid for any type of baths, be it phonons, particle-hole excitations, etc.

In the following, we derive the expressions of the T_1 and T_2 times resulting from the fluctuating field $\delta B_y(t)$. For this, we need to compute the bath correlator

$$J_{yy}(\omega) = \left(\frac{g\mu_B}{2\hbar}\right)^2 \int_0^\infty dt e^{-i\omega t}\langle \delta B_y(0)\delta B_y(t)\rangle, \quad (49)$$

where the brackets $\langle\cdots\rangle$ means tracing over the phonon bath being at thermal equilibrium at temperature T. The relaxation time within the Bloch-Redfield approach is given in the present particular case (the B field along the x direction) by (see Refs. 43 and 50),

$$T_1^{-1} = \mathrm{Re}(J_{yy}(\omega_Z^{eff}) + J_{yy}(-\omega_Z^{eff})), \quad (50)$$

with $\omega_Z^{eff} = E_Z^{eff}/\hbar$. Making use of Eq. (49), we then finally obtain for the relaxation rate

$$T_1^{-1} = T_{(0)1}^{-1}\left(\frac{\omega_Z^{eff}R}{c_l}\right)^5 \sum_s \left(\left|\frac{\partial q}{\partial \omega_{q,s}}\right| \frac{\mathcal{C}^2(q,s)}{\mathcal{F}(q,s)}\right)_{\omega_{q,s}\equiv\omega_Z^{eff}}, \quad (51)$$

where

$$T_{(0)1}^{-1} \approx 0.05\frac{\delta^2\hbar}{\rho_c R^5}\left(\frac{\Xi_0}{\Delta E_0}\right)^2\left(\frac{R}{\lambda_{SO}}\right)^2. \quad (52)$$

In the above expression, $\delta = E_Z/E_Z^{eff}$, and the functions $\mathcal{C}(q,s)$ and $\mathcal{F}(q,s)$ are defined in Eqs. (46) and (47). We mention that within first order in SOI, the decoherence time T_2 induced by phonons satisfies $T_2 = 2T_1$ since, as mentioned before, the fluctuating magnetic field induced by phonons $\boldsymbol{\delta B}$ is perpendicular to the applied one $\mathbf{B}$. In Fig. 2, we plot the relaxation time as a function of the ratio $\omega_Z^{eff}R/c_l$, for $R = 50$ nm and $c_l = 4\times10^3$ m/s. We see that the relaxation rate exhibits peaks as a function of the effective Zeeman splitting E_Z^{eff}. This is due to the finite size in the transverse direction which gives rise to phonon branches. Each new peak appears when E_Z^{eff} reaches a new energetically higher branch. Note that although the relaxation rate seems to diverge when reaching a new peak, in reality, this does not happen since there are many processes which broaden the phonon DOS at these special points, such as phonon-phonon scattering, phonon-substrate scattering, etc. The usual branch splitting is on the order of $\omega_{ph}^R \equiv c_l/R$, which stands for the phonon frequency in bulk material with the wave length equal to the dot size R. This frequency ω_{ph}^R (or energy, when expressed as $\hbar\omega_{ph}^R$) is the parameter which characterizes the dominant mechanism for the phonon-induced spin relaxation, which can be due to piezoelectric-potential or deformation-potential phonons. In the limit $\omega_Z^{eff} \ll \omega_{ph}^R$, the piezophonons give the main contribution to the relaxation rate T_1^{-1}, while in the opposite case, $\omega_Z^{eff} \gg \omega_{ph}^R$, the main contribution to the relaxation rate T_1^{-1} is given by deformation-potential phonons.[43] Here, we are in neither of the two limits, but in the range where Zeeman splitting is slightly larger than $\hbar\omega_{ph}^R$, i.e., $\omega_Z^{eff} \geqslant \omega_{ph}^R$. However, taking into account only the deformation-potential mechanism should give the right order of magnitude for the relaxation rate. We mention here that the relaxation rate T_1^{-1} in the low energy limit ($\omega_Z^{eff}R/c_l < 1$) is given predominantly by the longitudinal linear in q mode [$\omega_{long}(q) = c_l q$] and the bending mode, square in q [$\omega_{bend}(q) = Bq^2$, with B being a constant which depends on R].[47]

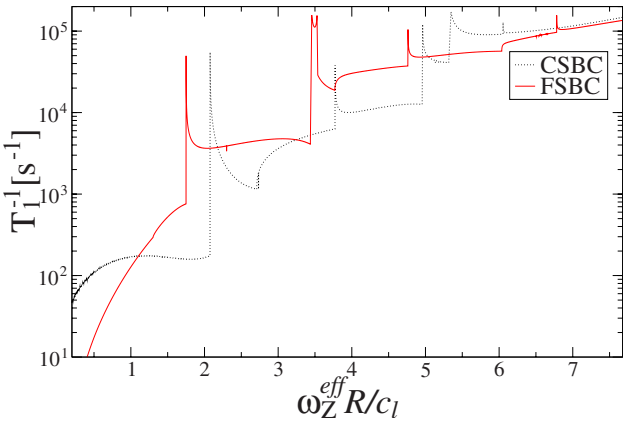

FIG. 2. (Color online) The relaxation rate T_1^{-1} as a function of the ratio $\omega_Z^{eff}R/c_l$ for both FSCBs and CSBCs (see text for explanations of FSBCs and CSBCs). Here, $\hbar c_l/R \simeq 0.6\times10^{-4}$ eV ($c_l \simeq 4\times10^3$ m/s and $R \simeq 50$ nm) corresponding to a magnetic field $B \simeq 0.2$ T for $g = 2.5$.

We see from Fig. 2 that each new phonon branch gives a strong enhancement of the relaxation rate T_1^{-1}, since it adds more phonon density of states. However, we see also that before the first peak, i.e., before reaching the first new branch, there is little spin relaxation ($T_1 \geqslant 10^{-3}$ s) for both FSBCs and CSBCs. This energy scale corresponds to a Zeeman splitting $E_Z^{eff} \approx 10^{-4}$ eV ($E_Z^{eff} \approx 1.2\times10^{-4}$ eV) for FSBCs (CSBCs).

If one tunes the *effective* Zeeman splitting E_Z^{eff} below the first peak, the relaxation rate of the qubit becomes very small, and the fact that E_Z^{eff} and *not* E_Z has to be tuned is practically an advantage for reasonably strong SOI since we need quite large E_Z for having large $g \propto E_Z$. In the present case, $E_Z^{eff}/E_Z \approx 0.93$, and for larger SOI, this ratio will be even smaller.

B. Spin relaxation in strongly transverse confined quantum dots

We give here a brief description of the phonon-induced spin relaxation for the case shown in Fig. 1(b). We first men-

tion that due to the strong confinement in the transverse direction, we can average the electron-phonon interaction over the transverse orbital ground state $|0_t\rangle$. Since for the ground-state wave function we have $m=0$ [see Eq. (25)], the only modes which couple to the electron, and thus eventually to the spin, are the $n=0$ modes of the phonon field in Eq. (40). Then, the problem of relaxation simplifies considerably.

The transformation $H_{e\text{-}ph}\to e^{-S}H_{e\text{-}ph}e^{S}$, with S given in Eq. (30), although exact, does not lead to a coupling of the spin to the phonon field since both the electron-phonon interaction Hamiltonian $H_{e\text{-}ph}$ and S contain only coordinate x operator, i.e., they commute. After this transformation, however, we are left with no SOI term, but with the x-dependent Zeeman coupling in Eq. (32). We now perform a second transformation $H_{e\text{-}ph}\to e^{-S'}H_{e\text{-}ph}e^{S'}$, with S' given before Eq. (33), under the assumption $E_Z\ll\hbar\omega_0$. Then, within first order in $E_Z/\hbar\omega_0$, we obtain for the spin-phonon Hamiltonian $H_{s\text{-}ph}$ the following expression:

$$H_{s\text{-}ph}=\langle 0|[S',H_{e\text{-}ph}]|0\rangle, \tag{53}$$

where we averaged also over the ground state $|0\rangle$ of the orbital Hamiltonian H_0. The spin-phonon Hamiltonian $H_{s\text{-}ph}$ reads

$$H_{s\text{-}ph}=\frac{1}{2}g\mu_B\delta B_{\tilde{x}}(t)\sigma_{\tilde{x}}+\frac{1}{2}g\mu_B\delta B_{\tilde{z}}(t)\sigma_{\tilde{z}}, \tag{54}$$

with

$$\delta B_{\tilde{x},\tilde{z}}(t)=B_{eff}\frac{\Xi_0}{\hbar\omega_0}\sum_{q,s}\frac{M^{\tilde{x},\tilde{z}}_{s\text{-}ph}(q)}{\sqrt{2\mathcal{F}(q,s)\rho_c\omega_{q,s}/\hbar}}K^2_{\boldsymbol{k}}b^\dagger_{\boldsymbol{k}}+\text{H.c.}, \tag{55}$$

and $\boldsymbol{k}\equiv\{q,s\}$. The functions $M^{\tilde{x},\tilde{z}}_{s\text{-}ph}$ are given by the following expressions:

$$M^{\tilde{x}}_{s\text{-}ph}(q)=\text{SinhInt}\left(\frac{l^2q}{\lambda_{SO}}\right), \tag{56}$$

$$M^{\tilde{z}}_{s\text{-}ph}(q)=\gamma-\text{CoshInt}\left(\frac{l^2q}{\lambda_{SO}}\right)+\log\left(\frac{l^2q}{\lambda_{SO}}\right), \tag{57}$$

where $\gamma=0.577$ is the Euler constant, $\log(x)$ is the natural logarithm, while the special functions $\text{SinhInt}(x)$ and $\text{CoshInt}(x)$ are defined as

$$\text{SinhInt}(x)=\int_0^x dt\frac{\sinh(t)}{t}, \tag{58}$$

$$\text{CoshInt}(x)=\gamma+\log(x)+\int_0^x dt\frac{\cosh(t)-1}{t}. \tag{59}$$

We see that there is both relaxation and pure dephasing of the spin due to spin-phonon interaction. However, since the deformation-potential phonons is super-Ohmic (even in 1D case for deformation-potential phonons), the pure dephasing rate vanishes[51] so that we retain in the following only the first term in Eq. (54). The relaxation rate T_1^{-1} can be found by the same procedure as in the previous case and reads

$$T_1^{-1}=\text{Re}(J_{\tilde{x}\tilde{x}}(\omega_Z^{eff})+J_{\tilde{x}\tilde{x}}(-\omega_Z^{eff})), \tag{60}$$

where the correlation function $J_{\tilde{x}\tilde{x}}$ is defined in Eq. (49) with $y\to\tilde{x}$, and $\omega_Z^{eff}=E_Z^{eff}/\hbar$, as before. The expression for the relaxation rate T_1^{-1} becomes

$$T_1^{-1}=T^{-1}_{(0)1}\left(\frac{\omega_Z^{eff}l}{c_l}\right)^5\sum_s\left(\left|\frac{\partial q}{\partial\omega_{q,s}}\right|\frac{\tilde{\mathcal{M}}^{2\tilde{x}}_{s\text{-}ph}(q)}{\mathcal{F}(q,s)}\right)_{\omega_{q,s}=\omega_Z^{eff}}, \tag{61}$$

where

$$T^{-1}_{(0)1}=\frac{\hbar}{2\pi\rho_cR^2l^3}\left(\frac{\Xi_0}{\hbar\omega_0}\right)^2 \tag{62}$$

and

$$\tilde{\mathcal{M}}^{\tilde{x}}_{s\text{-}ph}(q)=\mathcal{M}^{\tilde{x}}_{s\text{-}ph}(q)e^{-q^2l^2/8}. \tag{63}$$

In order to find now the dependence of the relaxation rate T_1^{-1} on the effective Zeeman splitting ω_Z^{eff}, we have to find first the phonon eigenfrequencies $\omega_{q,s}$. This can be done following the same steps as in the previous section, depending which kind of boundary conditions are used, i.e., FSBCs or CSBCs. As mentioned earlier, the average distance between the branches s is on the order of $\omega^R_{ph}=c_l/R$. Then, since $R\ll l$, and also due to the Gaussian suppression in Eq. (63), it is enough to consider in Eq. (61) only the lower branch $s=1$. If we now assume FSBCs and the limit $qR\ll 1$, the phonon eigenfrequency becomes linear in q, i.e., $\omega_{q,1}\equiv\omega(q)=c_sq$, with[47]

$$c_s=c_t\sqrt{\frac{3c_l^2-4c_t^2}{c_l^2-c_t^2}}. \tag{64}$$

The normalization function χ_0 acquires also a simple form in this limit and reads

$$\chi_0=\frac{c_l^2}{3c_l^2-4c_t^2}\frac{R}{q}\sqrt{\frac{\hbar}{2Mc_sq}}. \tag{65}$$

After inserting in Eq. (61) the expressions for $\omega(q)$ and χ_0, we obtain for the relaxation rate T_1^{-1} (FSBCs) the final expression

$$T_1^{-1}=\frac{T^{-1}_{(0)1}}{2}\left(\frac{c^2}{3c_l^2-4c_t^2}\right)^2\left(\frac{\omega_Z^{eff}l}{c_s}\right)^3\tilde{\mathcal{M}}^{\tilde{x}2}_{s\text{-}ph}(\omega_Z^{eff}l/c_s). \tag{66}$$

In Fig. 3, we plot the relaxation rate T_1^{-1} as a function of the dimensionless parameter $\omega_Z^{eff}l/c_s$ for different SOI strengths measured through the ratio l/λ_{SO}. We assumed here $R=10$ nm and $l=50$ nm, which give $\hbar c_s/l\equiv\hbar\omega^l_{ph}=0.05$ meV and $\hbar c_l/R\equiv\hbar\omega^R_{ph}=0.25$ meV. We see in Fig. 3 that the relaxation rate T_1^{-1} is quite large ($T_1^{-1}\sim 10^5$–10^7 s^{-1}) for $\omega_Z^{eff}/\omega^l_{ph}\sim 1$–$5$, i.e., when these energies are comparable. However, there is need for a large effective Zeeman splitting $E_Z^{eff}\gg\hbar\omega^l_{ph}$ to achieve a large spin-photon coupling $\mathcal{M}_\gamma$. At the same time, one should stay still below the next phonon branch, since above it, we find a substantial increase for the relaxation rate. Since this next phonon branch lies somewhere around $2\hbar\omega^R_{ph}\approx 0.5$ meV, the condition for efficient

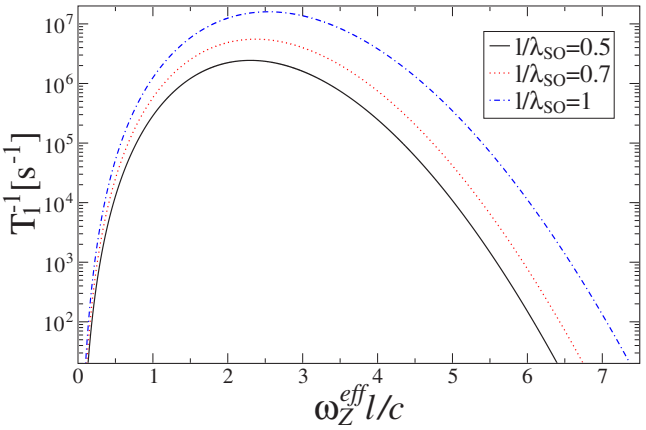

FIG. 3. (Color online) The relaxation rate T_1^{-1} as a function of the ratio $\omega_Z^{eff} l/c_s$ for three different ratios l/λ_{SO} and with FSBCs (see text).

spin-phonon coupling and weak relaxation becomes $\hbar\omega_{ph}^{l} \ll E_Z^{eff} < 2\hbar\omega_{ph}^{R}$. In this regime, we are actually satisfying also the necessary condition that $E_Z/\hbar\omega_0 \ll 1$, since for $l=50$ nm, we have $\hbar\omega_0=1.3$ meV. We mention that for CSBC the phonon spectrum is gapped, and, in consequence, there is no phonon-induced relaxation of the spin for Zeeman splittings E_Z^{eff} smaller than this gap Δ_{ph}. This energy (gap) is on the order of $\Delta_{ph} \sim 2\hbar\omega_{ph}^{R}=0.5$ meV. Note the nonmonotonic behavior of the relaxation rate as a function of the effective Zeeman splitting (see Fig. 3). This nonmonotonicity has the same origin as in GaAs QDs[43] and comes from the fact that for increasing Zeeman splitting, the wavelength of the phonon decreases, and when this becomes less than the dot length, the phonons decouple from the electron (i.e., the electron-phonon coupling averages to zero). A similar nonmonotonic effect has been recently observed in GaAs double QDs.[52]

C. Decoherence due to hyperfine interaction

The spin decoherence time due to single-phonon processes is given by $T_2=2T_1$ so that the main source for decoherence comes from the hyperfine interaction between the electron and the surrounding nuclei. This time scale T_2^* is given by[53,54]

$$T_2^* = 2\frac{\hbar\sqrt{N}}{A}, \tag{67}$$

where N is the number of nuclei in the sample and A is the hyperfine constant. The number of nuclei N can be found as

$$\frac{1}{N} = v_0 \int d^3\boldsymbol{r} |\psi(\boldsymbol{r})|^4, \tag{68}$$

where v_0 is the unit cell volume per nuclear spin and $\psi(\boldsymbol{r})$ is the wave function of the electron in the QDs. We see that the larger the number of nuclei, i.e., the bigger the dot, the longer the pure decoherence time T_2^* for the electron. In a typical GaAs QDs ($R=30$ nm and $l=5$ nm, $A_{\mathrm{GaAs}}=90$ μeV, and $N \approx 10^5$), this time scale is on the order of $T_2^* \sim 10^{-8}$ s.[53,54] In InAs material, the hyperfine constant $A_{\mathrm{InAs}} \approx 300$ μeV,[55] i.e., more than three times larger than in GaAs. However, the number of nuclei found from Eq. (68) is on the order $N \approx 10^6$ for both geometries so that the dephasing time $T_2^* \approx 4\times 10^{-9}$ s. However, again like in GaAs, we expect that coherently driving the qubit will prolong the T_2^* time up to 10^{-6} s and with echo up to 10^{-5} s.[16] Moreover, like in GaAs QDs, one can make use of state narrowing procedures,[56,57] which should lead to a further substantial enhancement of the decoherence time due to nuclear spins and possibly reach the SOI-induced limit of $10^{-1}-10^{-4}$ s calculated above for large magnetic field strengths.

IX. CONCLUSIONS

We have proposed and studied an efficient way to implement spin qubits localized in InAs nanowires coupled to a 1D electromagnetic transmission line (cavity) via SOI. We have analyzed two experimentally achievable configurations of the system. In the first case, the electronic confinement is much stronger along the nanowire axis than in the transverse direction (large-radius nanowires), while the other case corresponds to the opposite limit (small-radius nanowires). We have found an efficient coupling between the spin and the cavity modes due to strong vacuum fluctuations in the cavity and a sizable SOI in InAs. We also have shown that this spin-photon coupling can allow for coupling between two (or several) distant spins, depending on the detuning of the Zeeman splittings E_{iZ}^{eff} from the cavity mode $\hbar\omega$. The SOI-induced exchange coupling J between two spins can be controlled by electrical fields only, e.g., by changing the g factor and/or orbital level spacing. Also, single-spin rotations can be performed efficiently by electric fields only through the EDSR mechanism. Exploiting a stronger SOI in InAs nanowires than typically in GaAs structures might seemingly compromise the use of spin for quantum memory, because the orbital environment couples also stronger to the spin.

However, we have studied the relaxation of the spin due to the lattice vibrations in the InAs nanowires for both configurations and shown that the time scale for the spin decay is on the order of milliseconds for relatively strong magnetic fields ($B \sim 0.5-1$ T), much larger than the times associated with the spin-photon dynamics, which takes place on times scales on the order of $10^{-8}-10^{-7}$ s. This fact is due to the quasi-one-dimensional structure of the system where the phonon spectrum shows discrete branches, very different from the bulk limit.

We stress here also that the coupling of the quantized modes of the transmission line to the spin degree of freedom via SOI is not restricted to QDs in semiconductor nanostructures. In principle, this coupling should be possible in other spin-orbit coupled systems too, such as nitrogen-vacancy centers,[58,59] molecular magnets,[60–62] magnetic nanorings,[63] etc. In these systems, there is usually a large zero-field splitting of the lowest spin multiplet attributed to SOI or to dipole-dipole interaction. This would allow for an efficient coupling of the electric fields, quantum or classical, to the spin degree of freedom and finally providing a mechanism for an all-electrical implementation of spin-based quantum information processing.

As a final remark, we mention that the present scheme can be also used to form hybrid structures where spin qubits are integrated together with other types of qubits in the same 1D transmission line. For example, one can envision a setup where a spin qubit is coupled via the cavity modes to superconducting qubit as the one studied in Ref. 35 so that one can transfer arbitrary states between the two qubit systems.

ACKNOWLEDGMENTS

We thank D. Bulaev and G. Burkard for useful discussions. We acknowledge financial support from the Swiss NSF, the NCCR Nanoscience Basel, and JST ICORP.

APPENDIX: DISPLACEMENT AND STRESS TENSOR FOR CYLINDRICAL NANOWIRES

In this appendix, we give explicit formulas for the displacement $\boldsymbol{u}(\boldsymbol{r})$ and stress $\boldsymbol{t}(\boldsymbol{r})$ vectors, respectively. We can write the displacement vector $\boldsymbol{u}(\boldsymbol{r})=(u_r,u_\phi,u_z)$ from Eq. (41) in components

$$u_k(\boldsymbol{r},t)=\sum_j U_{kj}(r)\boldsymbol{\chi}_j e^{i(n\phi+qz-\omega t)},\quad k=r,\phi,z, \tag{A1}$$

with $\boldsymbol{\chi}_j=(\chi_0,\chi_1,\chi_2)$ and the matrix $\mathcal{U}(r)$ having the form

$$\mathcal{U}(r)=\begin{pmatrix} \frac{\partial}{\partial r}f_{0n}(r) & i\frac{n}{r}f_{1n}(r) & iq\frac{\partial}{\partial r}f_{2n}(r) \\ i\frac{n}{r}f_{0n}(r) & -\frac{\partial}{\partial r}f_{1n}(r) & -\frac{nq}{r}f_{2n}(r) \\ iqf_{0n}(r) & 0 & k_1^2 f_{2n}(r) \end{pmatrix}. \tag{A2}$$

The other relevant quantity for the elastic problem is the stress tensor T.[47] In order to obtain T, we first have to find the strain tensor S as a function of displacement $\boldsymbol{u}(\boldsymbol{r})$. The independent components of the strain tensor coordinates have expressions (in cylindrical coordinates)[47] of the form

$$S_{rr}=\frac{\partial u_r}{\partial r},$$

$$S_{\phi\phi}=\frac{1}{r}\left(\frac{\partial u_\phi}{\partial \phi}+u_r\right),$$

$$S_{zz}=\frac{\partial u_z}{\partial z},$$

$$S_{r\phi}=\frac{1}{2r}\left(\frac{\partial u_r}{\partial \phi}+r^2\frac{\partial}{\partial r}\left(\frac{u_r}{r}\right)\right),$$

$$S_{z\phi}=\frac{1}{r}\frac{\partial u_z}{\partial \phi}+\frac{\partial u_\phi}{\partial z},$$

$$S_{rz}=\frac{1}{2}\left(\frac{\partial u_r}{\partial z}+\frac{\partial u_z}{\partial r}\right). \tag{A3}$$

The stress tensor T, which quantifies the surface forces, is related to the strain tensor S by the elastic modulus constants.[47] Since we are interested in the boundary conditions at the surface of the cylinder, the relevant part of the stress tensor is given by the stress vector $\boldsymbol{t}=T\boldsymbol{e}_r$, with $\mathbf{e}_r$ being the unit vector along the radius. We write here only these relevant parts of the stress tensor T as a function of the strain tensor components,

$$T_{rr}=\rho(c_l^2-2c_t^2)(S_{rr}+S_{\phi\phi}+S_{zz})+2\rho c_t^2 S_{rr},$$

$$T_{r\phi}=2\rho c_t^2 S_{r\phi},$$

$$T_{rz}=2\rho c_t^2 S_{rz}, \tag{A4}$$

and $\boldsymbol{t}=(T_{rr},T_{r\phi},T_{rz})$. We write now the relevant stress vector $\boldsymbol{t}$, which is given explicitly by the following relation:

$$\begin{pmatrix} T_{rr} \\ T_{r\phi} \\ T_{rz} \end{pmatrix}=\rho\begin{pmatrix} c_l^2\frac{\partial}{\partial r}+(c_l^2-2c_t^2)\frac{1}{r} & (c_l^2-2c_t^2)\frac{1}{r}\frac{\partial}{\partial \phi} & (c_l^2-2c_t^2)\frac{\partial}{\partial z} \\ c_t^2\frac{1}{r}\frac{\partial}{\partial \phi} & c_t^2\left(\frac{\partial}{\partial r}-\frac{1}{r}\right) & 0 \\ c_t^2\frac{\partial}{\partial z} & 0 & c_t^2\frac{\partial}{\partial r} \end{pmatrix}\begin{pmatrix} u_r \\ u_\phi \\ u_z \end{pmatrix}. \tag{A5}$$

We can bring the stress matrix to the same form as we did for the displacement, namely, $t_k(\boldsymbol{r})=\Sigma_j \mathcal{T}_{kj}(r)\boldsymbol{\chi}_j e^{i(n\phi+qz-\omega t)}$, with the matrix $\mathcal{T}$ having the explicit form

$$\mathcal{T}(r) = \begin{pmatrix} \left(2c_t^2\frac{\partial^2}{\partial r^2} - (c_l^2 - 2c_t^2)\left(\frac{\omega}{c_l}\right)^2\right) f_{0n} & 2inc_t^2\frac{\partial}{\partial r}\left(\frac{f_{1n}}{r}\right) & 2iqc_t^2\frac{\partial^2}{\partial r^2} f_{2n} \\ 2inc_t^2\frac{\partial}{\partial r}\left(\frac{f_{0n}}{r}\right) & -c_t^2\left(2\frac{\partial^2}{\partial r^2} + k_1^2\right) f_{1n} & -2qnc_t^2\frac{\partial}{\partial r}\left(\frac{f_{2n}}{r}\right) \\ 2ic_t^2 q\frac{\partial}{\partial r} f_{0n} & -c_t^2\frac{nq}{r} f_{1n} & c_t^2(k_1^2 - q^2)\frac{\partial}{\partial r} f_{2n}. \end{pmatrix}. \quad \text{(A6)}$$

[1] D. Loss and D. P. DiVincenzo, Phys. Rev. A **57**, 120 (1998).
[2] V. Cerletti, W. A. Coish, O. Gywat, and D. Loss, Nanotechnology **16**, R27 (2005).
[3] R. Hanson, L. P. Kouwenhoven, J. R. Petta, S. Tarucha, and L. M. K. Vandersypen, Rev. Mod. Phys. **79**, 1217 (2007).
[4] M. A. Nielsen and I. L. Chuang, *Quantum Computation and Quantum Information* (Cambridge University Press, New York, 2000).
[5] C. Fasth, A. Fuhrer, L. Samuelson, V. N. Golovach, and D. Loss, Phys. Rev. Lett. **98**, 266801 (2007).
[6] M. T. Björk, A. Fuhrer, A. E. Hansen, M. W. Larsson, L. E. Froberg, and L. Samuelson, Phys. Rev. B **72**, 201307(R) (2005).
[7] L. P. Kouwenhoven, D. G. Austing, and S. Tarucha, Rep. Prog. Phys. **64**, 701 (2001).
[8] S. Tarucha, D. G. Austing, T. Honda, R. J. van der Hage, and L. P. Kouwenhoven, Phys. Rev. Lett. **77**, 3613 (1996).
[9] M. Ciorga, A. S. Sachrajda, P. Hawrylak, C. Gould, P. Zawadzki, S. Jullian, Y. Feng, and Z. Wasilewski, Phys. Rev. B **61**, R16315 (2000).
[10] J. M. Elzerman, R. Hanson, J. S. Greidanus, L. H. Willems van Beveren, S. De Franceschi, L. M. K. Vandersypen, S. Tarucha, and L. P. Kouwenhoven, Phys. Rev. B **67**, 161308(R) (2003).
[11] T. Hayashi, T. Fujisawa, H. D. Cheong, Y. H. Jeong, and Y. Hirayama, Phys. Rev. Lett. **91**, 226804 (2003).
[12] J. R. Petta, A. C. Johnson, C. M. Marcus, M. P. Hanson, and A. C. Gossard, Phys. Rev. Lett. **93**, 186802 (2004).
[13] J. M. Elzerman, R. Hanson, L. H. Willems van Beveren, B. Witkamp, L. M. K. Vandersypen, and L. P. Kouwenhoven, Nature (London) **430**, 431 (2004).
[14] S. Amasha, K. MacLean, I. Radu, D. M. Zumbuhl, M. A. Kastner, M. P. Hanson, and A. C. Gossard, arXiv:cond-mat/0607110, Phys. Rev. Lett. (to be published).
[15] A. C. Johnson, J. R. Petta, J. M. Taylor, A. Yacoby, M. D. Lukin, C. M. Marcus, M. P. Hanson, and A. C. Gossard, Nature (London) **435**, 925 (2005).
[16] J. R. Petta, A. C. Johnson, J. M. Taylor, E. A. Laird, A. Yacoby, M. D. Lukin, C. M. Marcus, M. P. Hanson, and A. C. Gossard, Science **309**, 2180 (2005).
[17] H.-A. Engel and D. Loss, Phys. Rev. B **65**, 195321 (2002).
[18] F. H. L. Koppens, C. Buizert, K. J. Tielrooij, I. T. Vink, K. C. Nowack, T. Meunier, L. P. Kouwenhoven, and L. M. K. Vandersypen, Nature (London) **442**, 766 (2006).
[19] K. C. Nowack, F. H. L. Koppens, Yu. V. Nazarov, and L. M. K. Vandersypen, Science **318**, 1430 (2007).
[20] V. N. Golovach, M. Borhani, and D. Loss, Phys. Rev. B **74**, 165319 (2006).
[21] E. A. Laird, C. Barthel, E. I. Rashba, C. M. Marcus, M. P. Hanson, and A. C. Gossard, arXiv:0707.0557 (unpublished).
[22] M. T. Björk, C. Thelander, A. E. Hansen, L. E. Jensen, M. W. Larsson, L. R. Wallenberg, and L. Samuelson, Nano Lett. **4**, 1621 (2004).
[23] C. Fasth, A. Fuhrer, M. T. Björk, and L. Samuelson, Nano Lett. **5**, 1487 (2005).
[24] A. Pfund, I. Shorubalko, R. Leturcq, and K. Ensslin, Appl. Phys. Lett. **89**, 252106 (2006).
[25] I. Shorubalko, A. Pfund, R. Leturcq, M. T. Borgström, F. Gramm, E. Müller, E. Gini, and K. Ensslin, Nanotechnology **18**, 044014 (2007).
[26] E. I. Rashba and Al. L. Efros, Phys. Rev. Lett. **91**, 126405 (2003).
[27] Y. Kato, R. C. Myers, A. C. Gossard, and D. D. Awschalom, Nature (London) **427**, 50 (2004).
[28] M. Duckheim and D. Loss, Nat. Phys. **2**, 195 (2006).
[29] M. Trif, V. N. Golovach, and D. Loss, Phys. Rev. B **75**, 085307 (2007).
[30] K. M. Svore, B. M. Terhal, and D. P. DiVincenzo, Phys. Rev. A **72**, 022317 (2005).
[31] A. Imamo$\bar{g}$lu, D. D. Awschalom, G. Burkard, D. P. DiVincenzo, D. Loss, M. Sherwin, and A. Small, Phys. Rev. Lett. **83**, 4204 (1999).
[32] J. Berezovsky, M. H. Mikkelsen, O. Gywat, N. G. Stoltz, L. A. Coldren, and D. D. Awschalom, Science **314**, 1916 (2006).
[33] M. Atature, J. Dreiser, A. Badolato, and A. Imamoglu, Nat. Phys. **3**, 101 (2007).
[34] A. Wallraff, D. I. Schuster, A. Blais, L. Frunzio, R.-S. Huang, J. Majer, S. Kumar, S. M. Girvin, and R. J. Schoelkopf, Nature (London) **431**, 162 (2004).
[35] A. Blais, R.-S. Huang, A. Wallraff, S. M. Girvin, and R. J. Schoelkopf, Phys. Rev. A **69**, 062320 (2004).
[36] O. Gywat, F. Meier, D. Loss, and D. D. Awschalom, Phys. Rev. B **73**, 125336 (2006).
[37] L. Childress, A. S. Sørensen, and M. D. Lukin, Phys. Rev. A **69**, 042302 (2004).
[38] G. Burkard and A. Imamoglu, Phys. Rev. B **74**, 041307(R) (2006).
[39] C. Cohen-Tannoudji, J. Dupont-Roc, and G. Grynberg, *Atom-Photon Interactions* (Wiley, New York, 1992).
[40] E. T. Jaynes and F. W. Cummings, Proc. IEEE **51**, 89 (1963).

[41] A. Blais, J. Gambetta, A. Wallraff, D. I. Schuster, S. M. Girvin, M. H. Devoret, and R. J. Schoelkopf, Phys. Rev. A **75**, 032329 (2007).
[42] I. L. Aleiner and V. I. Fal'ko, Phys. Rev. Lett. **87**, 256801 (2001).
[43] V. N. Golovach, A. Khaetskii, and D. Loss, Phys. Rev. Lett. **93**, 016601 (2004).
[44] L. S. Levitov and E. I. Rashba, Phys. Rev. B **67**, 115324 (2003).
[45] C. Flindt, A. S. Sorensen, and K. Flensberg, Phys. Rev. Lett. **97**, 240501 (2006).
[46] N. Nishiguchi, Phys. Rev. B **50**, 10970 (1994).
[47] A. N. Cleland, *Foundations of Nanomechanics: From Solid-State Theory to Devive Applications* (Springer-Verlag, Berlin, 2003).
[48] N. Nishiguchi, Phys. Rev. B **52**, 5279 (1995).
[49] M. A. Stroscio, K. W. Kim, Se Gi Yu, and A. Ballato, J. Appl. Phys. **76**, 4670 (1994).
[50] M. Borhani, V. N. Golovach, and D. Loss, Phys. Rev. B **73**, 155311 (2006).
[51] U. Weiss, *Quantum Dissipative Systems*, 2nd ed. (World Scientific, Singapore, 1998).
[52] T. Meunier, I. T. Vink, L. H. Willems van Beveren, K.-J. Tielrooij, R. Hanson, F. H. L. Koppens, H. P. Tranitz, W. Wegscheider, L. P. Kouwenhoven, and L. M. K. Vandersypen, Phys. Rev. Lett. **98**, 126601 (2007).
[53] A. V. Khaetskii, D. Loss, and L. Glazman, Phys. Rev. Lett. **88**, 186802 (2002).
[54] W. A. Coish and D. Loss, Phys. Rev. B **70**, 195340 (2004).
[55] T. Yokoi, S. Adachi, H. Sasakura, S. Muto, H. Z. Song, T. Usuki, and S. Hirose, Phys. Rev. B **71**, 041307(R) (2005).
[56] D. Klauser, W. A. Coish, and D. Loss, Phys. Rev. B **73**, 205302 (2006).
[57] D. Stepanenko, G. Burkard, G. Giedke, and A. Imamoglu, Phys. Rev. Lett. **96**, 136401 (2006).
[58] T. Gaebel *et al.*, Nat. Phys. **2**, 408 (2006).
[59] R. Hanson, F. M. Mendoza, R. J. Epstein, and D. D. Awschalom, Phys. Rev. Lett. **97**, 087601 (2006).
[60] M. N. Leuenberger and D. Loss, Nature (London) **410**, 789 (2001).
[61] J. Tejada, E. M. Chudnovsky, E. del Barco, J. M. Hernandez, and T. P. Spiller, Nanotechnology **12**, 181 (2001).
[62] J. Lehmann, A. Gaita-Ariño, E. Coronado, and D. Loss, Nat. Nanotechnol. **2**, 312 (2007).
[63] F. Troiani, A. Ghirri, M. Affronte, S. Carretta, P. Santini, G. Amoretti, S. Piligkos, G. Timco, and R. E. P. Winpenny, Phys. Rev. Lett. **94**, 207208 (2005).